EXIT-Chart Aided 3-Stage Concatenated Ultra-WideBand Time-Hopping Spread-Spectrum Impulse Radio Design

R. A. Riaz[1,2], R. G. Maunder[1], M. F. U. Butt[1,2], S. X. Ng[1], S. Chen[1] and L. Hanzo[1]
[1]School of ECS, University of Southampton, SO17 1BJ, United Kingdom.
Email: {rar06r, rm, mfub06r, sxn, sqc, lh}@ecs.soton.ac.uk, http://www-mobile.ecs.soton.ac.uk
[2]Dept of EE, COMSATS Institute of Information Technology, Islamabad, 44000, Pakistan, http://ciit.edu.pk

***Abstract*— A serially concatenated and iteratively decoded Irregular Variable Length Coding (IrVLC) scheme is amalgamated with a unity-rate precoded Time-Hopping (TH) Pulse Position Modulation (PPM) aided Ultra-Wide Bandwidth (UWB) Spread-Spectrum (SS) impulse radio design. The proposed design is capable of operating at low Signal-to-Noise Ratios (SNR) in Nakagami-m fading channels contaminated by Partial Band Noise Jamming (PBNJ) as a benefit of lossless IrVLC joint source and channel coding. Although this scheme may be readily used for lossless video or audio compression for example, we only used it here for lossless near-capacity data transmission. A number of component Variable Length Coding (VLC) codebooks having different coding rates are utilized by the IrVLC scheme for encoding specific fractions of the input source symbol stream. EXtrinsic Information Transfer (EXIT) charts are used to appropriately select these fractions in order to shape the inverted EXIT curve of the IrVLC and hence to match that of the inner decoder, which allows us to achieve an infinitesimally low Bit Error Ratio (BER) at near-capacity SNR values.**

I. INTRODUCTION

The novel contribution of this letter is that we advance the design of TH-PPM-UWB systems with the aid of sophisticated channel coding in the interest of approaching the attainable capacity. More specifically, our TH-PPM-UWB design exploits that analogous to Irregular Convolutional Coding (ICC) [1], the family of Irregular Variable Length Codes (IrVLC) [2] employs a number of component VLC codebooks having different coding rates [3] for encoding particular fractions of the input source symbol stream. The appropriate lengths of these fractions may be chosen with the aid of EXtrinsic Information Transfer (EXIT) charts [4] in order to shape the inverted EXIT curve of the IrVLC codec to ensure that it does not cross the EXIT curve of the inner channel codec. In this way, an open EXIT chart tunnel may be created even at near-capacity values of Signal-to-Noise Ratio (SNR).

UltraWideBand (UWB) communications systems are commonly defined as systems that have either more than 20 percent relative bandwidth compared to the band's center frequency or more than 500 MHz absolute bandwidth. The pioneering work of Win and Scholtz [5] developed the concept of Time-Hopping (TH) Pulse Position Modulation (PPM) UWB impulse radio systems. In the aforementioned systems, trains of time-shifted PPM pulses are used to transmit baseband or carrierless UWB signals.

Against this background, as a further contribution of this letter is that we extend the concept of classic 2-stage Extrinsic Information (EI) exchange [6] to a 3-stage UWB scheme constituted by a unity-rate decoder, an IrVLC decoder and the TH-PPM-UWB detector. Although this scheme may be readily used for loseless video or audio compression for example, we only used it here for loseless near-capacity data transmission. The technique of EXIT charts is utilized to investigate the serial concatenation of the TH-PPM-UWB detector, unity-rate decoder and an IrVLC outer decoder in order to attain a good performance even at near-capacity SNR values. We demonstrate that the 3-stage scheme outperforms the 2-stage benchmarker. The practical rationale of the proposed system is that of achieving lossless video or data file transmission in emerging high-rate USB-type applications, for example. Finally, a further novel aspect worthy of mentioning is that the system imposes the transmission efficiency by further compressing the source data.

This letter is organised as follows. In Sec. II, our complete system design philosophy is elaborated. In Sec. III, our EXIT chart and Bit Error Ratio (BER) results are discussed as a function of the IrVLC code parameters. Finally, in Sec. IV, we present our conclusions.

II. SYSTEM OVERVIEW

A. System Description

Our design considered in Fig. 1 assumes 16-ary VLC source symbol values obeying a 16-ary discrete probability density function (PDF) resulting from the Lloyd-Max (LM) quantization of independent Laplacian distributed source samples. The dynamic range of the symbol probabilities lies between 0.002 and 0.16, when considering 4-bit LM quantization. The entropy of the 16 symbols obeying these probabilities lies between 2.6 bits/symbol and 8.74 bits/symbol with an overall source entropy of 3.5 bits per VLC symbol. The rationale of

The financial support of the EPSRC UK, EU Optimix project is gratefully acknowledged.

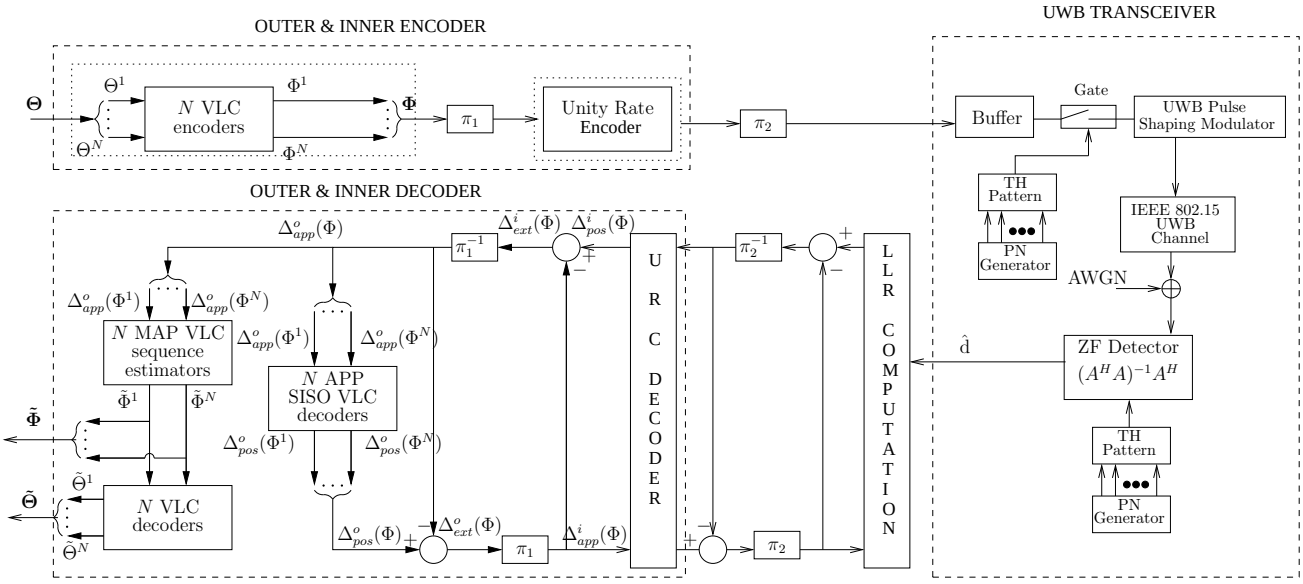

Fig. 1. Schematic of the IrVLC and VLC-based TH-PPM-UWB schemes. In the IrVLC coded scheme we have $N = 16$, whilst $N = 1$ in the VLC-coded scheme.

the proposed IrVLC coding scheme is that given this non-uniform probability of occurance for the 16 VLC symbols and their associated entropies, the VLC scheme is capable of data compression as well as of high-integrity detection at near-capacity SNRs.

The transmitter shown in Fig. 1 transmits the source symbol frame $\mathbf{\Theta}$, which comprises J number of source symbols having the $K = 16$-ary values $\{\Theta_j\}_{j=1}^{J} \in [1 \dots K]$. These source symbols are decomposed into N number of components $\{\mathbf{\Theta^n}\}_{n=1}^{N}$, where we opted for $N = 16$ in the case of the IrVLC-TH-PPM-UWB scheme considered and $N = 1$ in the case of the regular VLC-based benchmarker scheme. The number of symbols in the source symbol frame $\mathbf{\Theta}$, which is decomposed into the source symbol frame component $\mathbf{\Theta^n}$ is specified as J^n, where we have $J^1 = J$ in the case of the VLC-based scheme. By contrast, in the case of the IrVLC-based scheme, the specific values of $\{J^n\}_{n=1}^{N}$ may be appropriately chosen in order to shape the inverted EXIT curve of the IrVLC codec so that it does not cross the EXIT curve of the precoder as detailed in [7].

Each of the N source symbol frame components $\{\mathbf{\Theta^n}\}_{n=1}^{N}$ is VLC-encoded using the corresponding codebook from the set of N VLC codebooks $\{\mathbf{VLC}^n\}_{n=1}^{N}$, having a range of coding rates $\{R^n\}_{n=1}^{N} \in [0, 1]$. The specific source symbols having the value of $k \in [1 \dots K]$ and encoded by the specific VLC codebook $\mathbf{VLC}^n$ are represented by the codeword $\mathbf{VLC}^{n,k}$, which has a length of $I^{n,k}$ bits. The J^n number of VLC codewords that represent the J^n number of source symbols in the source symbol frame component $\mathbf{\Theta^n}$ are concatenated to provide the transmission frame component $\mathbf{\Phi^n} = \{\mathbf{VLC}^{n,\Theta_{j^n}^n}\}_{j^n=1}^{J^n}$.

Depending on the specific length of the VLC codewords, the number of bits comprised by each transmission frame component $\mathbf{\Phi^n}$ will typically vary slightly from frame to frame. In order to facilitate the VLC decoding of each transmission frame component $\mathbf{\Phi^n}$, it is necessary to explicitly convey its length $I^n = \sum_{j^n=1}^{J^n} I^{n,s_{j^n}^n}$ to the receiver with the aid of side information. The N transmission frame components $\{\mathbf{\Phi^n}\}_{n=1}^{N}$ encoded by the different IrVLC component codes are concatenated at the transmitter, as shown in Fig. 1. The resultant transmission frame $\mathbf{\Phi}$ has a length of $\sum_{n=1}^{N} I^n$ bits. Following the bit interleaver π_1, the transmission frame $\mathbf{\Phi}$ is precoded and then interleaved again by the bit interleaver π_2. The interleaved bits are sent to the buffer depicted in Fig. 1. These bits are transmitted by the TH-PPM modulator.

The transmitter shown in Fig. 1 transmits the source symbol frame $\mathbf{\Theta}$, which comprises J number of source symbols having the $K = 16$-ary values $\{\Theta_j\}_{j=1}^{J} \in [1 \dots K]$. These source symbols are decomposed into N number of components $\{\mathbf{\Theta^n}\}_{n=1}^{N}$, where we opted for $N = 16$ in the case of the IrVLC-TH-PPM-UWB scheme considered and $N = 1$ in the case of the regular VLC-based benchmarker scheme. The number of symbols in the source symbol frame $\mathbf{\Theta}$, which is decomposed into the source symbol frame component $\mathbf{\Theta^n}$ is specified as J^n, where we have $J^1 = J$ in the case of the VLC-based scheme. By contrast, in the case of the IrVLC-based scheme, the specific values of $\{J^n\}_{n=1}^{N}$ may be appropriately chosen in order to shape the inverted EXIT curve of the IrVLC codec so that it does not cross the EXIT curve of the precoder as detailed in [7].

Each of the N source symbol frame components $\{\mathbf{\Theta^n}\}_{n=1}^{N}$ is VLC-encoded using the corresponding codebook from the set of N VLC codebooks $\{\mathbf{VLC}^n\}_{n=1}^{N}$, having a range of coding rates $\{R^n\}_{n=1}^{N} \in [0, 1]$. The specific source symbols having the value of $k \in [1 \dots K]$ and encoded by the specific VLC codebook $\mathbf{VLC}^n$ are represented by the codeword $\mathbf{VLC}^{n,k}$, which has a length of $I^{n,k}$ bits. The J^n number of VLC codewords that represent the J^n number of source symbols in the source symbol frame component $\mathbf{\Theta^n}$ are concatenated to provide the transmission frame component $\mathbf{\Phi^n} = \{\mathbf{VLC}^{n,\Theta_{j^n}^n}\}_{j^n=1}^{J^n}$.

Depending on the specific length of the VLC codewords, the

number of bits comprised by each transmission frame component $\mathbf{\Phi^n}$ will typically vary slightly from frame to frame. In order to facilitate the VLC decoding of each transmission frame component $\mathbf{\Phi^n}$, it is necessary to explicitly convey its length $I^n = \sum_{j^n=1}^{J^n} I^{n,s^n_{j^n}}$ to the receiver with the aid of side information. The N transmission frame components $\{\mathbf{\Phi^n}\}_{n=1}^{N}$ encoded by the different IrVLC component codes are concatenated at the transmitter, as shown in Fig. 1. The resultant transmission frame $\mathbf{\Phi}$ has a length of $\sum_{n=1}^{N} I^n$ bits. Following the bit interleaver π_1, the transmission frame $\mathbf{\Phi}$ is precoded and then interleaved again by the bit interleaver π_2. The interleaved bits are sent to the buffer depicted in Fig. 1. These bits are transmitted by the TH-PPM modulator.

B. UWB Transmission and Detection

TH-PPM-UWB: A general TH-PPM-UWB signal is given by

$$g(t) = \sum_{n=-\infty}^{\infty} \phi(t - nT_F - T_{PP_n} - T_{CH_n}), \tag{1}$$

where $\phi(t)$ is the signalling pulse shape, T_F is the frame duration, T_{PP_n} is the PPM-related shift in the pulse position, either forward or backward with respect to the nominal signalling instant to represent the binary stream, T_{CH_n} is the time shift based on the unique user-specific TH code reminiscent of the Pseudo-Noise (PN) sequence of a specific user, where the code repeats after a certain interval. The frame duration T_F is typically of the order of 1000 times the actual pulse width to avoid any inter-symbol interference (ISI) imposed by multipath propagation.

Channel Model: The Channel Impulse Response (CIR) ratified by the IEEE 802.15.3 standard and considered here can be expressed as [8]

$$h(t) = \sum_{l=1}^{L} h_l e^{j\varphi_l} \delta(t - lT_\varphi), \tag{2}$$

where L represents the number of resolvable paths, while h_l and φ_l are the gain and phase of the lth resolvable CIR tap. Furthermore, lT_φ represents the corresponding delay of the lth CIR tap. As shown in [9], [10] the CIR taps of the UWB channel follow Nakagami distribution, which has been validated by using the Kolmogorov-Smirnov testing at a significance level of 1%. We assume in our analysis that the phase rotation imposed by the channel is uniformly distributed in $[0, 2\pi]$. The transmitted signal is also corrupted both by Additive White Gaussian Noise (AWGN) and Partial Band Noise Jamming (PBNJ) having single-sided power spectral densities of N_0 and N_J, respectively.

Zero Forcing Detector (ZFD): The data estimates $\hat{\mathbf{d}}$ at the output of the ZFD are:

$$\hat{\mathbf{d}}_{\mathbf{ZFD}}\Big|_{\mathbf{R}_n=\sigma^2 I} = (\mathbf{A^H A})^{-1}\mathbf{A^H y}. \tag{3}$$

where $\mathbf{n}$ is the noise sequence, which has a covariance matrix of $\mathbf{R}_n = E[nn^H]$, $\mathbf{A}$ is the overall system matrix. Eq (3) assumes that $\mathbf{n}$ consists of noise samples that are zero-mean Gaussian variables having a variance of σ^2 with the corresponding covariance matrix $\mathbf{R}_n = \sigma^2 I$, where I is the identity matrix [11]. After the ZFD, the corresponding symbol probabilities and log-likelihood ratios (LLRs) are computed, which are then fed to the unity-rate decoder of Fig. 1.

C. Iterative Decoding

The conditional probability of the jth transmitted symbol Θ_j, where $j = 0, \ldots, J-1$, given the signal $\hat{\mathbf{d}} = \left[d_0, d_1, \ldots, d_{J-1}\right]$, which represents the set of J outputs of the ZFD in Fig. 1 is given by

$$P(\Theta_j|\hat{\mathbf{d}}) = \frac{p(\hat{\mathbf{d}}|\Theta_j)P(\Theta_j)}{p(\hat{\mathbf{d}})}, \tag{4}$$

where $p(\hat{\mathbf{d}}|\Theta_j)$ is the PDF of the received signal $\hat{\mathbf{d}}$, given that Θ_j is transmitted. Furthermore, $P(\Theta_j)$ is the *a priori* probability of the symbol Θ_j, while $p(\hat{\mathbf{d}}) = \sum_{j=0}^{J-1} p(\hat{\mathbf{d}}|\Theta_j)P(\Theta_j)$ is the probability of receiving the signal set $\hat{\mathbf{d}}$. At the first iteration we have $P(\Theta_j) = 1/J$ for all the transmitted symbols, since no *a priori* information is available. The PDF $p(\hat{\mathbf{d}}|\Theta_j)$ uniquely determines the statistics required for estimating the probability $P(\Theta_j|\hat{\mathbf{d}})$. The expression of $p(\hat{\mathbf{d}}|\Theta_j)$ is given by

$$p(\hat{\mathbf{d}}|\Theta_j) = f_{d_j}(v_j|\Theta_j) \prod_{x=0, x\neq j}^{J-1} f_{d_n}(v_x|\Theta_j), \tag{5}$$

where $f_{d_n}(v_x|\Theta_j)$ represents the PDF of the xth detector value, $x = 0, 1, \ldots, J-1$, given that Θ_j is transmitted. The simplified expression for $p(\hat{\mathbf{d}}|\Theta_j)$ is

$$p(\hat{\mathbf{d}}|\Theta_j) = \exp\left(\frac{v_j\gamma_h}{1+\gamma_h}\right), \tag{6}$$

where $\gamma_h = bRE_b/(N_0L)$ is the SNR per hop, R is the code rate, E_b is the transmitted energy per bit and $b = \log_2 M$ is the number of bits per symbol. The corresponding Log-Likelihood Ratios (LLRs) [4] can be computed from Eqs. (5) and (6).

The derivation of the soft information from the received signal is different for the 2-stage and 3-stage serial concatenated schemes. In the first case, the unity-rate *a posteriori probability* (APP) Soft-Input-Soft-Output (SISO) decoder and the outer decoder exchange EI in order to perform Iterative Detection (ID), both invoking the Bahl-Cocke-Jelinek-Raviv (BCJR) algorithm using bit-based trellises. Again, we refer to this ID-aided configuration as the *2-stage scheme*. Alternatively, the system may be modified so that the TH-PPM-UWB detector, the unity-rate inner decoder and the IrVLC outer decoder exchange their EI, as shown in Fig. 1. We refer to this arrangement as the *3-stage scheme*. The 3-stage scheme requires the additional interleaver π_2 between the precoder and the TH-PPM-UWB detector of Fig. 1.

Since N separate VLC encoders are employed in the TH-PPM-UWB transmitter, N separate VLC decoders have to be used in the corresponding receiver seen in Fig. 1. In parallel to the composition of the bit-based transmission frame $\mathbf{\Phi}$ from N VLC source symbols, the *a priori* LLRs $\Delta^o_{app}(\mathbf{\Phi})$ are decomposed into N components, as shown in Fig. 1, although each of the components processes a proportionely reduced number of symbols. Hence the associated complexity is increased only modestly. This is achieved with the aid of the explicit side information that we assume to be available

for conveying the slightly varying number of bits I^n of each transmission frame component $\mathbf{\Phi^n}$. Each of the N number of VLC decoders is provided with the *a priori* LLR sub-frame $\Delta^o_{app}(\mathbf{\Phi^n})$ and in response it generates the *a posteriori* LLR sub-frame $\Delta^o_{pos}(\mathbf{\Phi^n})$, $n \in [1 \dots N]$. These *a posteriori* LLR sub-frames are concatenated in order to provide the *a posteriori* LLR frame $\Delta^o_{pos}(\mathbf{\Phi})$.

During the final decoding iteration, N bit-based Maximum Aposteriori Probability (MAP) VLC sequence estimation processes are invoked instead of single-class APP SISO VLC decoding, as shown in Fig. 1. In this case, each transmission frame component $\mathbf{\Phi^n}$ is estimated from the corresponding *a priori* LLR frame component $\Delta^o_{app}(\mathbf{\Phi^n})$. The resultant transmission frame component estimates $\tilde{\mathbf{\Phi}}^{\mathbf{n}}$ may be concatenated to provide the transmission frame estimate $\tilde{\mathbf{\Phi}}$. Additionally, the transmission frame component estimates $\tilde{\mathbf{\Phi}}^{\mathbf{n}}$ may be VLC decoded to provide the source symbol frame component estimates $\tilde{\mathbf{\Theta}}^{\mathbf{n}}$.

III. Performance Analysis

We have used $N = 16$-component VLC codebooks $\{\mathbf{VLC}^n\}_{n=1}^N$ having approximately equally spaced coding rates in the range of $[0.2, 0.95]$ in the TH-PPM-UWB scheme. Moreover, unless otherwise stated, we employ the following parameter values: source symbol frame length of $J = 80,000$, outer code rate of $R = 0.5$, TH-PPM-UWB spreading factor of $M = 16$ and a diversity order of $L = 3$. In each case, we employ a Variable Length Error Correcting (VLEC) codebook [3] that is tailored to the source symbol values' probabilities of occurrence. Again, these codes compress the unequal probability input data symbols for the sake of achieving a near-entropy source-rate and a lower probability at near-capacity SNRs. By contrast, in the VLC benchmarker scheme, we employ just $N = 1$ VLC codebook, which is identical to the VLC codebook $\mathbf{VLC}^{10}$ of the IrVLC scheme, having a coding rate of $R = 0.5$. Note that this coding rate results in an average interleaver length of $J \cdot \frac{E}{R}$ bits. The inverted EXIT curve of

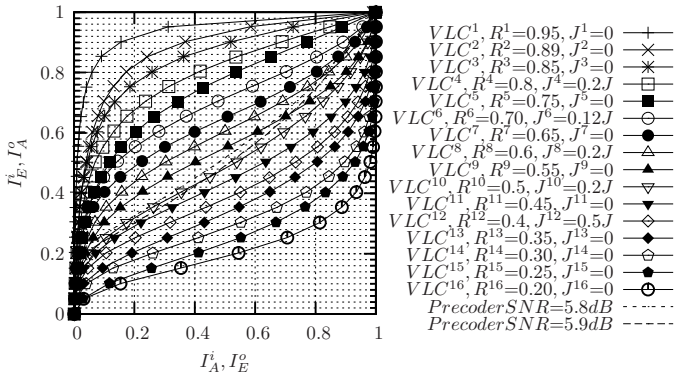

Fig. 2. Inverted VLC EXIT curves and unity rate decoder EXIT curves assuming uncorrelated Nakagami-m fading channel.

the IrVLC scheme is also shown in Fig. 2, assuming an uncorrelated Nakagami-m fading channel contaminated by PBNJ characterised by $\frac{E_b}{N_J} = 10$dB and a jamming factor of $\rho = 0.1$. This was obtained as the appropriately weighted superposition of the $N = 16$ component VLC codebooks' inverted EXIT curves, where the weight applied to the inverted EXIT curve of the component VLC codebook $\mathbf{VLC^n}$ is proportional to the specific number of source symbols employed for encoding J^n [1]. Using the approach of [1], the values of $\{J^n\}_{n=1}^N$ given in Fig. 2 were designed so that the IrVLC, composite coding rate matches that of our regular VLC benchmarker scheme, namely 0.5. Furthermore, we ensured that the inverted IrVLC EXIT curve did not cross the unity-rate decoder's EXIT curve at $\frac{E_b}{N_0}$ of 5.9dB. We note that only 4 of the 16 VLC components were indeed activated by the algorithm of [1] in order to encode a non-zero number of source symbols. As shown in Fig. 2, the presence of an open EXIT chart tunnel implies that an infinitesimally low BER may be achieved by the TH-PPM-UWB scheme for $\frac{E_b}{N_0}$ values above 5.9dB. By contrast, an open EXIT chart tunnel is not afforded for $\frac{E_b}{N_0}$ values below 5.8dB in the case of the VLC-based benchmarker scheme.

TABLE I

Parameter values for the IrVLC based concatenated schemes.

Channel	S	Convergence Min. Value				$\alpha_n = \frac{J^n}{J}$ values
		IrVLC		VLC		
		The.	Act.	The.	Act.	
Interf. free	2	5.7	5.7	5.9	5.9	[0,0,0,0.18,0,0.12,0, 0.18,0,0,0,0.52,0,0,0,0]
	3	4.7	4.8	5.0	5.1	[0,0,0,0.26,0,0.24,0,0, 0,0,0,0.34,0.13,0.03,0,0]
$\frac{E_b}{N_J}$=10 ρ=0.1	2	6.6	6.7	6.9	7	[0,0,0,0.24,0,0,0,0.22, 0,0.03,0,0.5,0,0,0,0]
	3	5.8	5.9	6.1	6.2	[0,0,0,0,0.18,0,0.27,0,0, 0,0,0,0.55,0,0,0,0]
$\frac{E_b}{N_J}$=10 $\rho = 0.5$	2	9.4	10.4	9.8	10.7	[0,0,0,0.08,0,0.16,0.11, 0,0,0.5,0,0,0,0,0,0]
	3	6.8	7.5	7.9	8.7	[0,0,0,0.13,0,0.32,0,0, 0,0,0,0.55,0,0,0,0]

Analogous to the IrVLC design of Fig. 2, we have also designed IrVLC codes for both the 2-stage and 3-stage ID aided scheme, assuming various jamming scenarios in Nakagami-m fading channels. The design parameter values are listed in Table I, where the relevant minimum values of $\frac{E_b}{N_0}(dB)$ or $\frac{E_b}{N_J}(dB)$ at which an open convergence tunnel is formed are shown alongside the specific fractions of the source symbol frame encoded by each component code of the IrVLC scheme given by $\alpha_n = \frac{J^n}{J}$. Both the EXIT-chart based as well as the Monte-Carlo simulation-based convergence-SNR values are shown in Table I for both the IrVLC and the VLC schemes. Here the theoretical values imply those predicted by the EXIT chart analysis, while the actual values are those achieved in the symbol-by-symbol Monte Carlo simulations. The code rates of the IrVLC's component codes used in our simulations are $[0.95, 0.89, 0.85, 0.8, 0.75, 0.7, 0.65, 0.6, 0.55, 0.5, 0.45, 0.4, 0.35, 0.3, 0.25, 0.2]$.

Fig. 3 provides the BER performance of both the 2-stage and the 3-stage schemes versus $\frac{E_b}{N_J}$, assuming $\frac{E_b}{N_0}$=10 dB and ρ=0.5. It becomes explicit from Fig. 3 that the 3-stage scheme yields an improvement of nearly 3 dB over the 2-stage IrVLC. The performance gain achieved by the 3-stage scheme is at the expense of a slightly higher complexity, imposed by the extra interleaver and decoder. Fig. 3 demonstrates

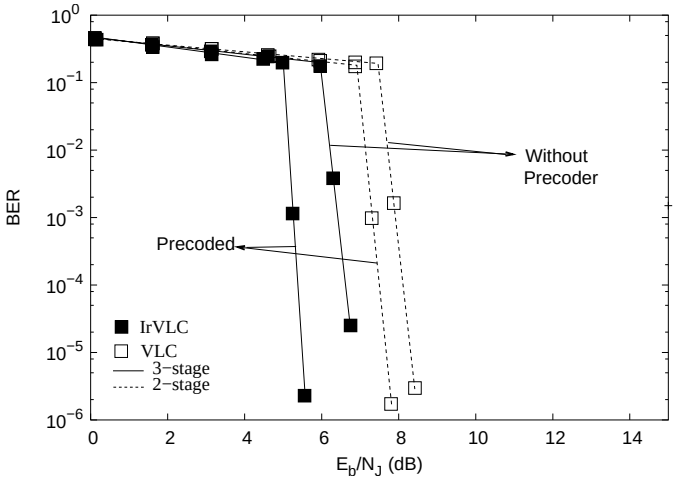

Fig. 3. BER versus $\frac{E_b}{N_J}$ performance of the 2-stage and 3-stage VLC and IrVLC based schemes in jammed, uncorrelated Nakagami-m fading channels assuming $\frac{E_b}{N_o}$=10 dB and ρ=0.5.

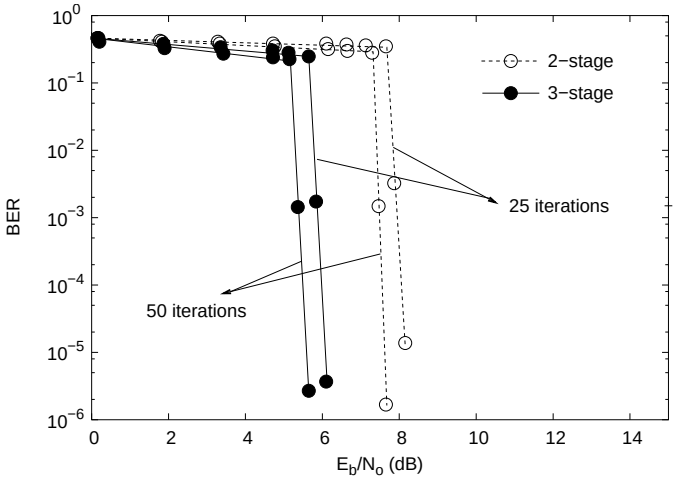

Fig. 4. BER versus $\frac{E_b}{N_o}$ performance of the 2-stage and 3-stage VLC and IrVLC based schemes in jammed, uncorrelated Nakagami-m fading channels assuming $\frac{E_b}{N_J}$=10 dB and ρ=0.1.

that the 3-stage scheme outperforms the corresponding VLC-based arrangement by 1.1 dB. The effect of reducing the number of iterations in both the 2-stage and 3-stage schemes is characterized in Fig. 4. Finally, Fig. 5 portrays the EXIT curves of the IrVLC and unity-rate decoders as well as the corresponding decoding trajectory, assuming an interference free, uncorrelated Nakagami-m fading channel for an SNR of 5.9dB.

IV. Conclusion

In this treatise we have investigated the serial concatenation of IrVLC coding with a TH-PPM-UWB design operating in a Nakagami-m fading channel in conjunction with PBNJ. Consequently, we noted that the precoder-aided scheme yields a gain of more than 6.9 dB over the system operating without a precoder. An open EXIT chart tunnel may be created at low SNR values. Moreover, the proposed 3-stage design performs 2.9 dB better than the corresponding 2-stage scheme.

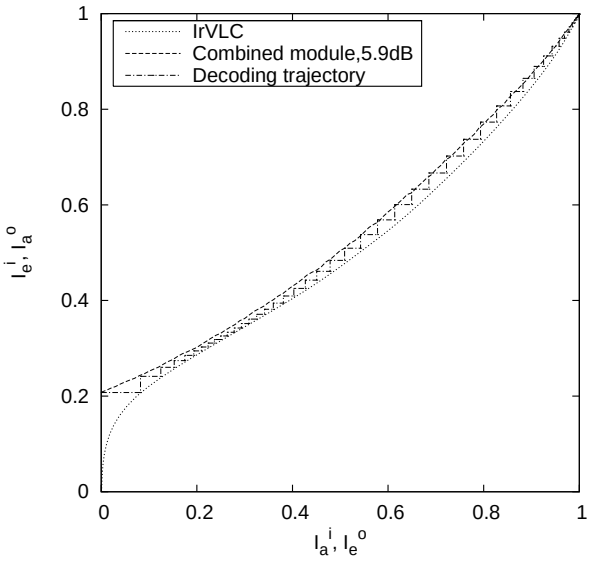

Fig. 5. IrVLC and Unity-rate decoders EXIT curves as well as decoding trajectory, assuming jammed, uncorrelated Nakagami-m fading channels with ρ=0.1.

References

[1] M. Tüchler and J. Hagenauer, "EXIT charts of irregular codes," in *Conference on Information Sciences and Systems*, Princeton, NJ, March 2002, pp. 748–753.

[2] R. G. Maunder, J. Wang, S. X. Ng, L. L. Yang, and L. Hanzo, "On the performance and complexity of irregular variable length codes for near-capacity joint source and channel coding," *IEEE Transactions on Wireless Communications*, vol. 7, no. 4, pp. 1338–1347, Apr. 2008.

[3] V. Buttigieg and P. G. Farrell, "Variable-length error-correcting codes," *IEE Proceedings on Communications*, vol. 147, no. 4, pp. 211–215, August 2000.

[4] S. ten Brink, "Convergence of iterative decoding," *IEEE Transactions on Communications*, vol. 49, no. 10, pp. 1727 – 1737, October 2001.

[5] M. Z. Win and R. A. Scholtz, "Impulse radio: how it works," *IEEE Communications Letters*, vol. 2, no. 2, pp. 36–38, Feb. 1998.

[6] C. Berrou, A. Glavieux, and P. Thitimajshima, "Near Shannon limit error correcting coding and decoding: Turbo codes," *IEEE Transactions on Communications*, pp. 1064–1070, 1993.

[7] L. Hanzo, P. Cherriman, and J. Streit, *Video Compression and Communications: From Basics to H.261, H.263, H.264, MPEG4 for DVB and HSDPA-Style Adaptive Turbo-Transceivers*. England: John Wiley and Sons, England, 2007.

[8] H. Sato and T. Ohtsuki, "Frequency domain channel estimation and equalisation for direct sequence ultra wideband (DS-UWB) system," *IEE Proceedings- Communications*, vol. 153, no. 1, pp. 93–98, Feb. 2006.

[9] A. F. Molisch, "Ultrawideband propagation channels-theory, measurement, and modeling," *IEEE Transactions on Vehicular Technology*, vol. 54, no. 5, pp. 1528–1545, Sept. 2005.

[10] R. A. Riaz, M. F. U. Butt, S. Chen, and L. Hanzo, "Generic z-domain discrete-time transfer function estimation for ultra-wideband systems," *Electronics Letters*, vol. 44, pp. 1491–1492, Dec. 2008.

[11] L. Hanzo, L.-L. Yang, E.-L. Kuan, and K. Yen, *Single- and Multi-Carrier DS-CDMA: Multi-User Detection, Space-Time Spreading, Synchronisation, Networking and Standards*. New York: John Wiley and Sons, England, 2003.